

A discrete adjoint-based level set topology optimization method for stress and buckling constraints

Hao Deng*, and Kazuhiro Saitou

Department of Mechanical Engineering, University of Michigan, Ann Arbor, MI 48109

*Corresponding author. Email: kazu@umich.edu

Abstract

This paper proposes a new sensitivity computational scheme for velocity field level set method with discrete adjoint method. The velocity field of level set method is described in B-spline space. The adjoint equations are constructed based on discretized governing equations. This paper demonstrates that the velocity field of level set method can be fully derived from the discrete adjoint method. This enables the circumvention of shape sensitivity analysis for standard level set method. We demonstrate the effectiveness of proposed method in the context of stress and linearized buckling topology optimization problems.

Keywords: Topology optimization, velocity-field level set method, discrete adjoint sensitivities, stress constraints, buckling constraints.

1. Introduction

Continuum topology optimization has become an important tool to determine the optimal shape for maximum performance subject to given design constraints. After three decades since the first development of Homogenization Design Method (HMD) [1], several topology optimization methods have been proposed, such as, density-based method [2], level set method [3], BESO method [4] and more recently, moving morphable components (MMC) [5-7], moving morphable voids (MMV) [8], and geometry projection method [9-11].

The Level set method (LSM) is a class of shape and topology optimization method, where the topology of a structure is described implicitly using the level set function ϕ , with the boundary defined by $\{\phi = 0\}$. A comprehensive literature review for level set methods in topology optimization can be found in Ref [12]. In classical LSM, the boundary is updated through evolving the implicit function ϕ based on Hamilton-Jacobi equation in which the optimization problem needs to be transformed in an unconstrained problem by Lagrangian formulations. During the optimization, the Lagrangian multipliers are gradually updated based on a certain strategy to improve convergence. The evolution of the implicit level set function is driven by normal velocity of the boundary $\{\phi = 0\}$ based on natural velocity extension [13] or the fast-marching method [14]. Besides the classical LSM formulation, the parametric level-set method has drawn great attention in recent years. Wang et al [15] proposed an Radial Basis Function (RBF) level set optimization method to transform the Hamilton-Jacobi equation into a system of ordinary differential equations (ODEs) based on a collocation formulation. Since then, several parametric level-set methods [16-19] with different basis functions for various physical problems have been proposed. In a velocity field level-set (VFLS) method [20, 21] recently proposed by Wang et al, the parametric boundary normal velocity field is defined to derive the level set function, instead of the parametric level set function deriving the boundary normal velocity as conventionally formulated. The velocity field is controlled by prescribed basis functions and velocity design variables at given points in the design domain. VFLS method provides an effective way to

handling multiple constraints and enables the use of the standard mathematical programming algorithms. In [22], Wang et al incorporated the topological derivative concept into VFLS method to enable the automatic nucleation of interior holes.

For classical LSM for topology optimization, the continuous adjoint method is widely used to compute sensitivities [13]. One of the major obstacles of continuous adjoint method is the sensitivity expressions are discontinuous at the nodes and edges of finite elements. In general, interpolation and smoothing techniques are needed to avoid discontinuity with a price of reduced the accuracy of the resulting sensitivity. Such interpolation and smoothing may even lead to divergence for high move limits as demonstrated by Kambampati et al [23]. Compared to the continuous adjoint method that follows the “differentiate-then-discretize” scheme [24], the discrete adjoint method follows the “discretize-then-differentiate” scheme, where the partial differential equations are first discretized using finite element method. The discretized equations are then differentiated to obtain adjoint equations based on augmented functional equations. While the discretize adjoint method has been widely used in density-based topology optimization methods [25], Kambampati et al [23] introduced the discrete adjoint method into the classical LSM for the first time using a semi-analytical formulation, where the boundary is perturbed implicitly to obtain level set sensitivity (*i.e.*, velocity) based on finite difference approximation.

This paper presents an analytical formulation for the discrete adjoint sensitivity in LSM-based topology optimization, which, for the first time, links the discrete adjoint method in the classical LSM with the normal boundary velocity. The proposed analytical formulation allows the normal boundary velocity of a level set to be is analytically derived from the discrete adjoint method, circumventing shape sensitivity analysis while eliminating any potential sources of numerical errors. The effectiveness of the proposed formulation is demonstrated in the VFLS-based topology optimization using B-Spline basis considering stress and local buckling constraints.

The remainder of the paper is organized as follows. Section 2 presents the mathematical formulation of B-spline VFLS based on discrete adjoint method. Section 3 demonstrates two typical topology optimization problems with local stress and buckling constraints. Section 4 concludes the paper with discussion of possible future directions.

2. B-spline Velocity Field Level Set Topology Optimization Method

2.1 Definition of B-spline velocity field level set (VFLS) function

In LSM, the material domain Ω at time t during the optimization within fixed design domain D can be represented by a signed distance function $\Phi(\mathbf{x}, t)$:

$$\begin{cases} \Phi(\mathbf{x}, t) > 0 & \text{if } \mathbf{x} \in \Omega \setminus \partial\Omega \\ \Phi(\mathbf{x}, t) = 0 & \text{if } \mathbf{x} \in \partial\Omega \cap D \\ \Phi(\mathbf{x}, t) < 0 & \text{if } \mathbf{x} \in D \setminus \Omega \end{cases} \quad (1)$$

The shape and topology of material domain Ω evolve over a course of time through moving its boundary $\partial\Omega$, which is realized by solving the Hamilton-Jacobi equation with velocity V^n in the normal direction of $\partial\Omega$:

$$\frac{\partial\Phi}{\partial t} - V^n |\nabla\Phi| = 0 \quad (2)$$

For $D \subset \mathbb{R}^2$, we can construct normal velocity field $V^n(\mathbf{x}, t)$ using a piece-wise function as follows,

$$V^n(\mathbf{x}, y, t) = \sum_{j=1}^{n_K} V_j(t) p_j(\mathbf{x}, y) \quad (3)$$

where V_j is design variables. n_K is the number of design variable points (velocity knots). In this paper, the velocity knots are selected as the centroid of FEM element. A special piecewise function is utilized here to work as basis function,

$$p_j(\mathbf{x}) = \begin{cases} 1 & \|\mathbf{x}\|_\infty \leq r \\ 0 & \|\mathbf{x}\|_\infty > r \end{cases} \quad (4)$$

For 2D square mesh, $r = 0.5L$ is selected for computation, where L is element length. Based on this special piecewise basis, the velocity field inside each element is a constant and only depends on the velocity at the centroid of element. This special piecewise function brings a simplification for sensitivity computation, which will be elaborated in the following section. The value at velocity knots can be described in B-spline space as follows,

$$V(x, y, t) = \sum_{k=0}^{n_x} \sum_{l=0}^{n_y} B_{k,p}(x) B_{l,q}(y) b_{k,l}(t) \quad (5)$$

where $B_{k,p}: \mathbb{R} \rightarrow \mathbb{R}$ $B_{l,q}: \mathbb{R} \rightarrow \mathbb{R}$ ($k = 0, 1, \dots, n_x; l = 0, 1, \dots, n_y$) are B-spline basis functions defined by knot vectors in x and y directions, respectively, p and q are the degrees of the B-spline basis functions, and $b_{k,l}(t)$ is a B-spline coefficient [26]. Once the velocity field is obtained by Eq. (3) and Eq. (5) for a given value of $b_{k,l}(t)$ at time t during optimization, level set function $\Phi(\mathbf{x}, t)$ can be updated through Eq. (2) using, for example, the upwind difference scheme [14] and the method of moving asymptotes (MMA) algorithm [27]. Then, the re-initialization step is implemented to avoid numerical deterioration of the level set function. More implementation details can be found in Ref [20].

2.2 Sensitivity analysis based on discrete adjoint method

The analytical derivation of the normal velocity field V^n from the discrete adjoint method is presented in two steps. First, we introduce the derivation of the discrete adjoint sensitivity for the density-based method [28]. Second, using the chain rule, we relate the sensitivity with respect to B-spline velocity coefficients with the discrete adjoint sensitivity with respect to the density obtained in the first step.

Step 1: The discretized governing equation for linear elastic problem can be written as follows,

$$\Psi = \mathbf{K}\mathbf{u} - \mathbf{f} = \mathbf{0} \quad (6)$$

where \mathbf{K} is the stiffness matrix, \mathbf{u} is the displacement vector, and \mathbf{f} is the nodal force vector. Note that any other constraint equations for physical problems are written as follows,

$$\mathcal{H} = \mathbf{0} \quad (7)$$

For a given objective function F , an augmented Lagrangian function is defined as follows,

$$G = F + \boldsymbol{\psi}^T \Psi + \boldsymbol{\kappa}^T \mathcal{H} \quad (8)$$

where $\boldsymbol{\psi}$ and $\boldsymbol{\kappa}$ are Lagrange multipliers. The sensitivity of augmented Lagrangian function G with respect to discretized density field $\boldsymbol{\rho}$ within D can be expressed as follows,

$$\frac{\partial G}{\partial \boldsymbol{\rho}} = \frac{\partial F}{\partial \boldsymbol{\rho}} + \boldsymbol{\psi}^T \frac{\partial \Psi}{\partial \boldsymbol{\rho}} + \boldsymbol{\kappa}^T \frac{\partial \mathcal{H}}{\partial \boldsymbol{\rho}} \quad (9)$$

where Lagrange multiplier should satisfy,

$$\boldsymbol{\psi}^T \frac{\partial \Psi}{\partial \boldsymbol{\rho}} + \boldsymbol{\kappa}^T \frac{\partial \mathcal{H}}{\partial \boldsymbol{\rho}} + \frac{\partial F}{\partial \boldsymbol{\rho}} = \mathbf{0} \quad (10)$$

The above derivation is usually referred to as the discrete adjoint method.

Step 2: Based on the chain rule,

$$\frac{\partial F}{\partial b_{k,l}} = \sum_{i=1}^{n_e} \frac{\partial F}{\partial \rho_i} \frac{\partial \rho_i}{\partial b_{k,l}} \quad (11)$$

The first term $\frac{\partial F}{\partial \rho_i}$ in the right-hand side of Eq. (11) can be obtained by Eq. (9). Based on the chain rule, the second term $\frac{\partial \rho_i}{\partial b_{k,l}}$ can be written as,

$$\frac{\partial \rho_i}{\partial b_{k,l}} = \sum_{j=1}^{n_v} \frac{\partial \rho_i}{\partial V_j^n} \frac{\partial V_j^n}{\partial b_{k,l}} \quad (12)$$

where V_j^n and ρ_i denote the normal velocity at velocity point j in $\partial\Omega$ and the density at element i in D , respectively, and n_e is the number of finite elements in D . n_v denotes the number of velocity point in $\partial\Omega$. The first term $\frac{\partial \rho_i}{\partial V_j^n}$ in the right-hand side of Eq. (12) represents the change in the volume fraction (density) of element i due to the change in the normal velocity point j . Dissimilar to Kambampati *et al* [23], where implicit perturbation near the boundary point is applied to numerically approximate the second term $\frac{\partial \rho_i}{\partial V_j^n}$ using the finite difference method, in this paper we analytically derive $\frac{\partial \rho_i}{\partial V_j^n}$ without a numerical approximation. Since $\rho_i = H(\Phi_i)$ where $H(\cdot)$ is Heaviside function [3], the chain rule yields:

$$\frac{\partial \rho_i}{\partial V_j^n} = \frac{\partial H(\Phi_i)}{\partial V_j^n} = \delta(\Phi_i) \cdot \frac{\partial \Phi_i}{\partial V_j^n} \quad (13)$$

where $\delta(x) \equiv \frac{\partial H(x)}{\partial x}$ is Dirac function [3]. Here, as mentioned in Eq. (3) and Eq. (4), the i th element density ρ_i is only dependent on the velocity knot value V_i^n of i th element. Thus Eq. (10) can be rewritten as,

$$\frac{\partial \rho_i}{\partial V_j^n} = \delta(\Phi_i) \cdot \delta_{ij} \frac{\partial \Phi_i}{\partial V_j^n} \quad (14)$$

where $\delta_{ij} = 1$ if $j = i$, otherwise $\delta_{ij} = 0$. In order to obtain $\frac{\partial \Phi_i}{\partial V_i^n}$, Eq. (2) is rewritten as:

$$d\Phi_i - V_i^n |\nabla \Phi_i| dt = 0 \quad (i = 1, 2, \dots, n_v) \quad (15)$$

where dt is a pseudo time, $\Phi_i \equiv \Phi(\mathbf{x}_i, t)$, $V_i^n \equiv V^n(\mathbf{x}_i, t)$. Now let δV_i^n be a small perturbation of velocity V_i^n and $\delta \Phi_i$ be the corresponding variation of $d\Phi_i$. Ignoring the effect of small perturbation $\delta \Phi_i$ on $|\nabla \Phi_i|$, Eq (15) becomes:

$$(d\Phi_i + \delta \Phi_i) - (V_i^n + \delta V_i^n) |\nabla \Phi_i| dt = 0 \quad (16)$$

which can be simplified as:

$$\delta \Phi_i - \delta V_i^n |\nabla \Phi_i| dt = 0 \quad (17)$$

Therefore,

$$\frac{\partial \Phi_i}{\partial V_i^n} = |\nabla \Phi_i| dt \quad (18)$$

Note that the pseudo time dt here can be regarded as 1, because the dt would be just a scaling factor of sensitivity $\frac{\partial F}{\partial V_j^n}$ which will not have any effect on optimization progress if the optimization algorithm is capable of adjusting move limits at each iteration, such as the method of moving asymptotes (MMA) [27].

$$\frac{\partial \rho_i}{\partial b_{k,l}} = \sum_{j=1}^{n_v} \frac{\partial \rho_i}{\partial V_j^n} \frac{\partial V_j^n}{b_{k,l}} \quad (19)$$

Substituting Eq. (18) and Eq. (14) into Eq. (12) with $dt = 1$ and using Eq. (5), we have

$$\frac{\partial \rho_i}{\partial b_{k,l}} = \delta(\Phi_i) \cdot |\nabla \Phi_i| \sum_{j=1}^{n_v} \left(\delta_{ij} B_{k,p}(x_j) B_{l,q}(y_j) \right) \quad (20)$$

Assuming the velocity points are located at the centroid of each element i with $\delta(\Phi_i) \neq 0$ (*i.e.*, boundary element), Eq. (20) can be simplified as:

$$\frac{\partial \rho_i}{\partial b_{k,l}} = \delta(\Phi_i) |\nabla \Phi_i| B_{k,p}(x_i) B_{l,q}(y_i) \quad (21)$$

where (x_i, y_i) is the coordinates of the centroid of boundary element i . Substituting this to Eq. (11), the sensitivity of function F with respect to B-spline coefficient $b_{k,l}$ can be given as:

$$\frac{\partial F}{\partial b_{k,l}} = \sum_{i=1}^{n_e} \frac{\partial F}{\partial \rho_i} \delta(\Phi_i) |\nabla \Phi_i| B_{k,p}(x_i) B_{l,q}(y_i) \quad (22)$$

2.3 Topology Optimization Problem Formulation

In the examples in the next section, the B-spline velocity field level set topology optimization is formulated as the volume minimization subject to stress and local buckling constraints. The optimization problem can be formulated as,

$$\begin{aligned} & \min V \\ & \text{s. t. } \sigma^{PM} \leq \sigma^* \\ & \text{s. t. } KS[\mu_i]_{(i \in \mathbb{Z})} \leq \mu^* \end{aligned} \quad (23)$$

where σ^{PM} and σ^* respectively denote the p-norm stress and its upper limit for constraining the maximum stress, and $KS[\mu_i]_{(i \in \mathbb{Z})}$ and μ^* respectively denote the KS aggregation and its upper bound for guarding against buckling. The reader should refer to [29] and [30] for the mathematical formulation and derivation of the sensitivities for these constraints, which are summarized also in Appendix A. While these formulations are given as a function of element density ρ_i , the sensitivities with respect to B-spline coefficients $b_{k,l}$ of velocity field can be readily derived based on the mathematical formulation in Eq. (22). In the following examples, parameters p and γ (refer to Appendix A) are set as 8 and 50, respectively.

4. Numerical Examples

4.1 Compressed square design

The first example considers a compressed square design, as illustrated in Fig. 1. The square is discretized by 300×300 finite elements with unit element length. The elastic modulus of the material is $E = 1$, and Poisson's ratio is chosen as $\nu = 0.3$. The bounds of the velocity design variables are selected as ± 0.2 , and the moving limit of MMA algorithm is 0.2. The B-spline knots are uniformly distributed in the design domain with a fixed interval Δ as shown in Fig. 1. The initialization of level set function is shown in Fig. 2. The optimization terminates once the relative difference of the target function between two adjacent iterations is smaller than 10^{-4} .

4.1.1 Volume minimization with p-norm stress constraint

The objective is minimizing the volume fraction with the p-norm stress constraint only (*i.e.*, no buckling constraint). The load is uniformly distributed at the middle of the top surface and has total magnitude $|F| = 1$. The upper bound of p-norm stress σ^* is set to be $\sigma^* = 1.3$. In this simple example, we will examine the effect of knot number on optimal topology design. Three different B-spline knot span lengths Δ are applied, and the corresponding optimized structures are shown in Figs. 3-5. The lowest volume fraction ($V = 0.075$) is reached if $\Delta = 0.01L$, where L is the length of the sides of the square. Compared to the larger value of knot span length ($\Delta = 0.04L$), it can be seen that more design freedom is achieved with small Δ .

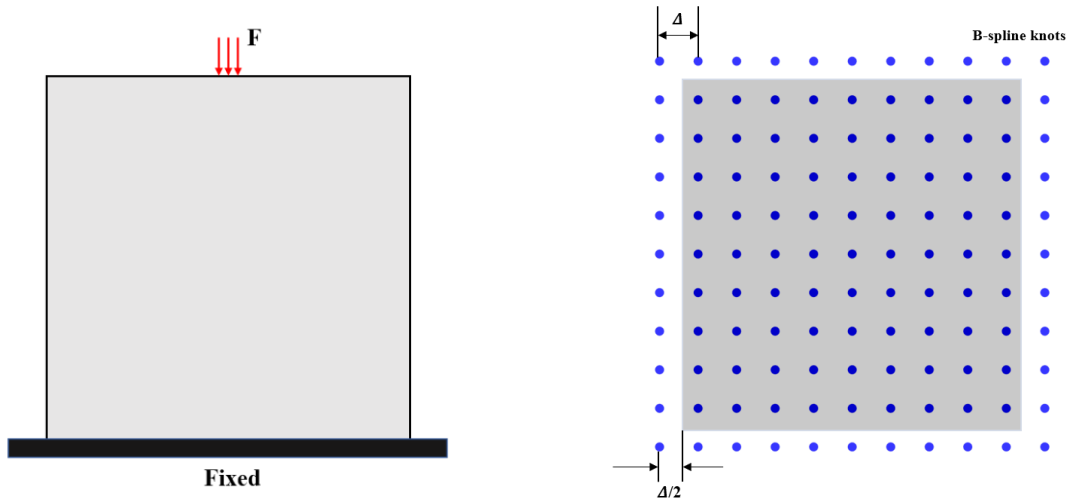


Figure 1. Compressed square design.

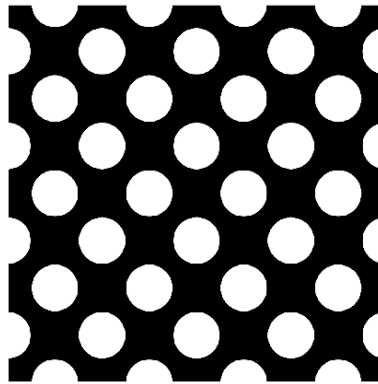


Figure 2. Level set initialization.

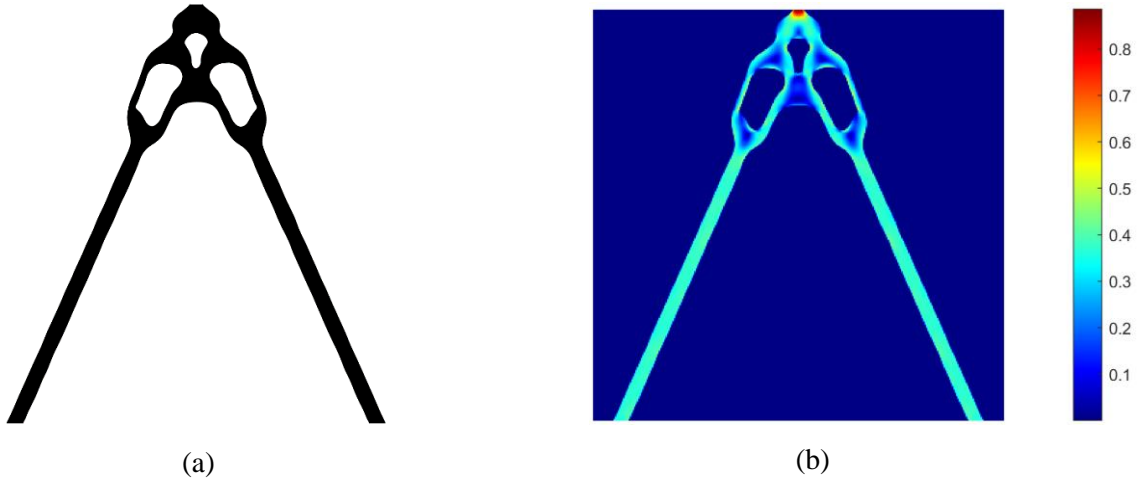


Figure 3. Optimized result: (a) material layout; (b) von Mises stress distribution ($V = 0.09, \Delta = 0.04L$).

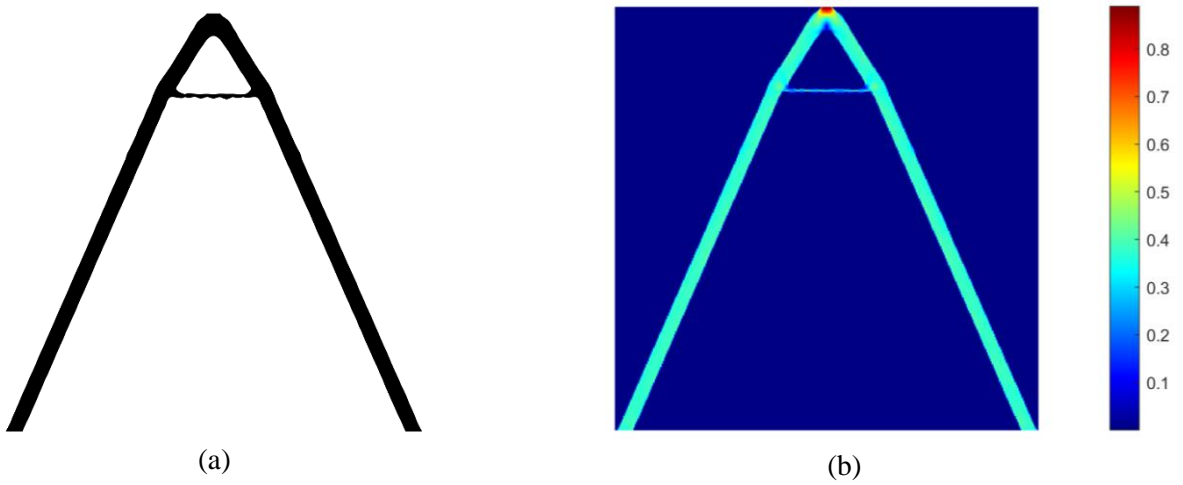


Figure 4. Optimized result: (a) material layout; (b) von Mises stress distribution ($V = 0.078, \Delta = 0.02L$).

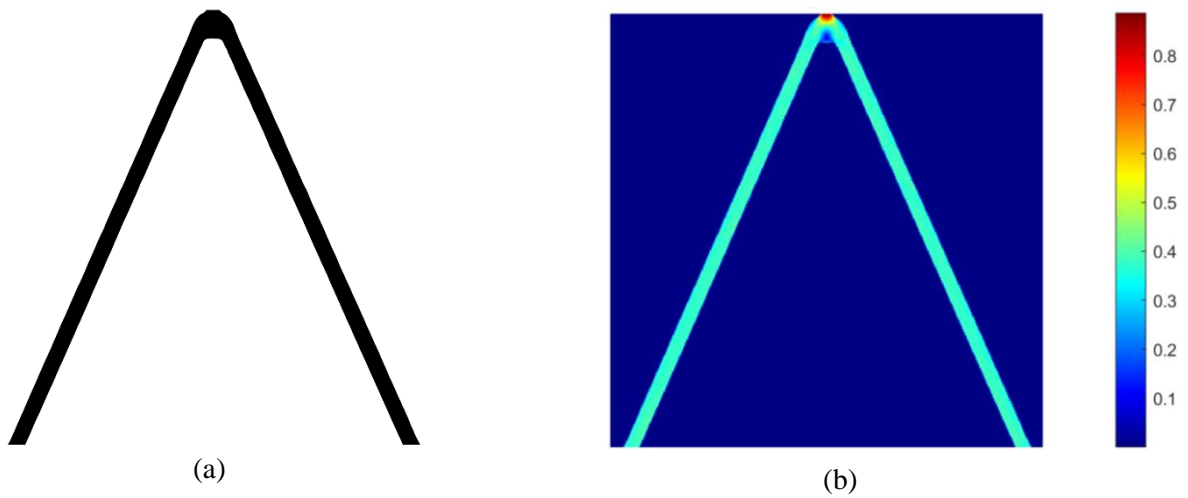


Figure 5. Optimized result: (a) material layout (b) von Mises stress distribution ($V = 0.075, \Delta = 0.01L$).

4.1.2 Volume minimization with buckling constraint

The objective is minimizing the volume fraction with fundamental buckling load constraint only (*i.e.*, no maximum stress constraint). The force is uniformly distributed on the four nodes at the mid of the upper edge. The total force magnitude is $|F| = 10^{-3}$. The buckling constraint μ^* is set to be $\mu^* = 0.15$. The B-spline knot span length is chosen as $\Delta = 0.01L$. Fig. 6 shows the optimized design. Fig. 7 shows the convergence history of the objective function (volume fraction) and left-hand side of the buckling constraint. The volume fraction decreases steadily until convergence is achieved. Because the fundamental buckling load need to be computed through solving eigenvalue problem, which is highly sensitivity to boundary movement, some local small fluctuations are seen in optimization. The volume fraction of designs decreases from 0.61 to 0.201 after 500 iterations.

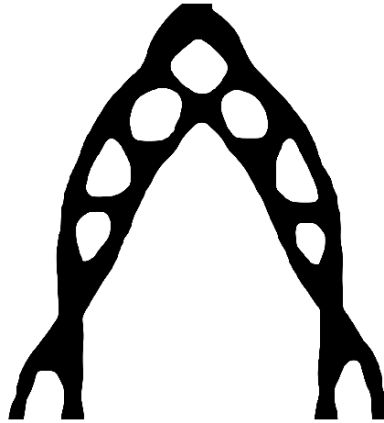


Figure 6. optimized design.

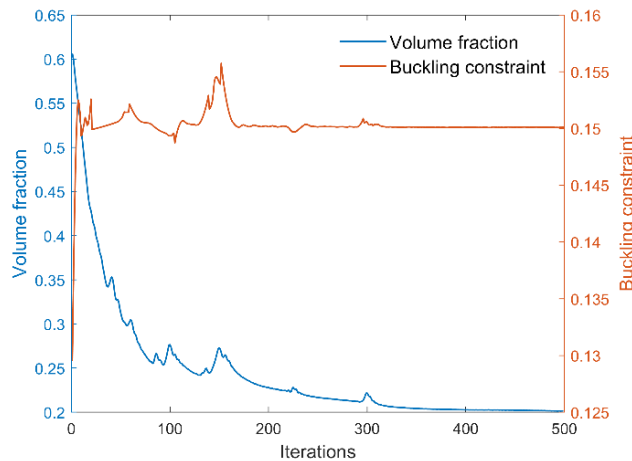


Figure 7. Convergence history of buckling constraint design.

4.1.3 Volume minimization with buckling and stress constraint

This example applies both volume minimization with stress and buckling load constraints. Similar to the previous examples, the constraint for p-norm stress σ^* and buckling constraint μ^* are set to be $\sigma^* = 1.3$ and $\mu^* = 0.15$. Correspondingly, the loading force on the mid upper surface for stress and buckling are the same as sections 4.1.1 and 4.1.2, respectively. The optimized design is shown in Fig. 8(a) and the von Mises distribution is shown in Fig. 8(b). Fig. 9 presents the evolution of material layout. Due to the buckling load constraint, no slender beam structures are found in final design. The convergence history is shown in Fig.

10. The volume fraction decreases steadily from initial value nearby 0.6 to 0.216 during optimization.

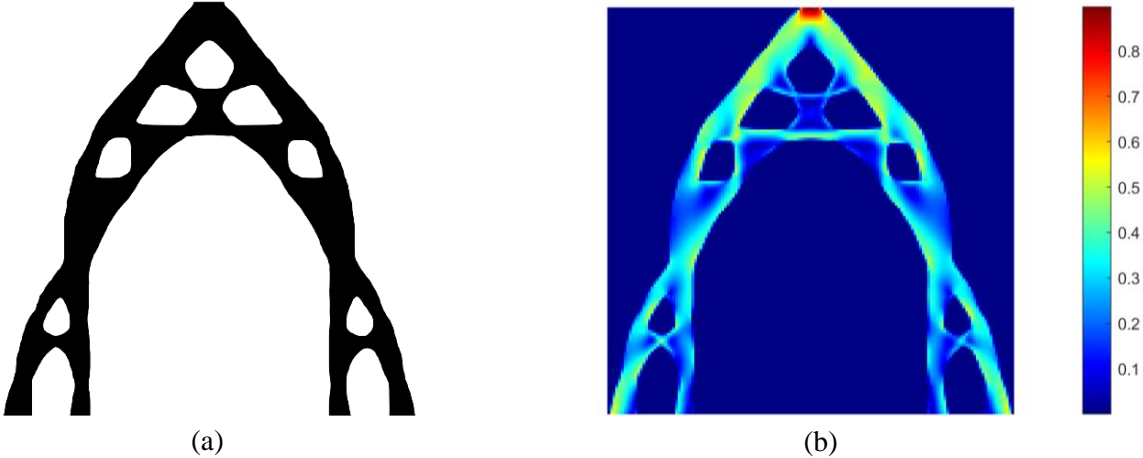


Figure 8. Optimized result: (a) material layout; (b) von Mises stress distribution.

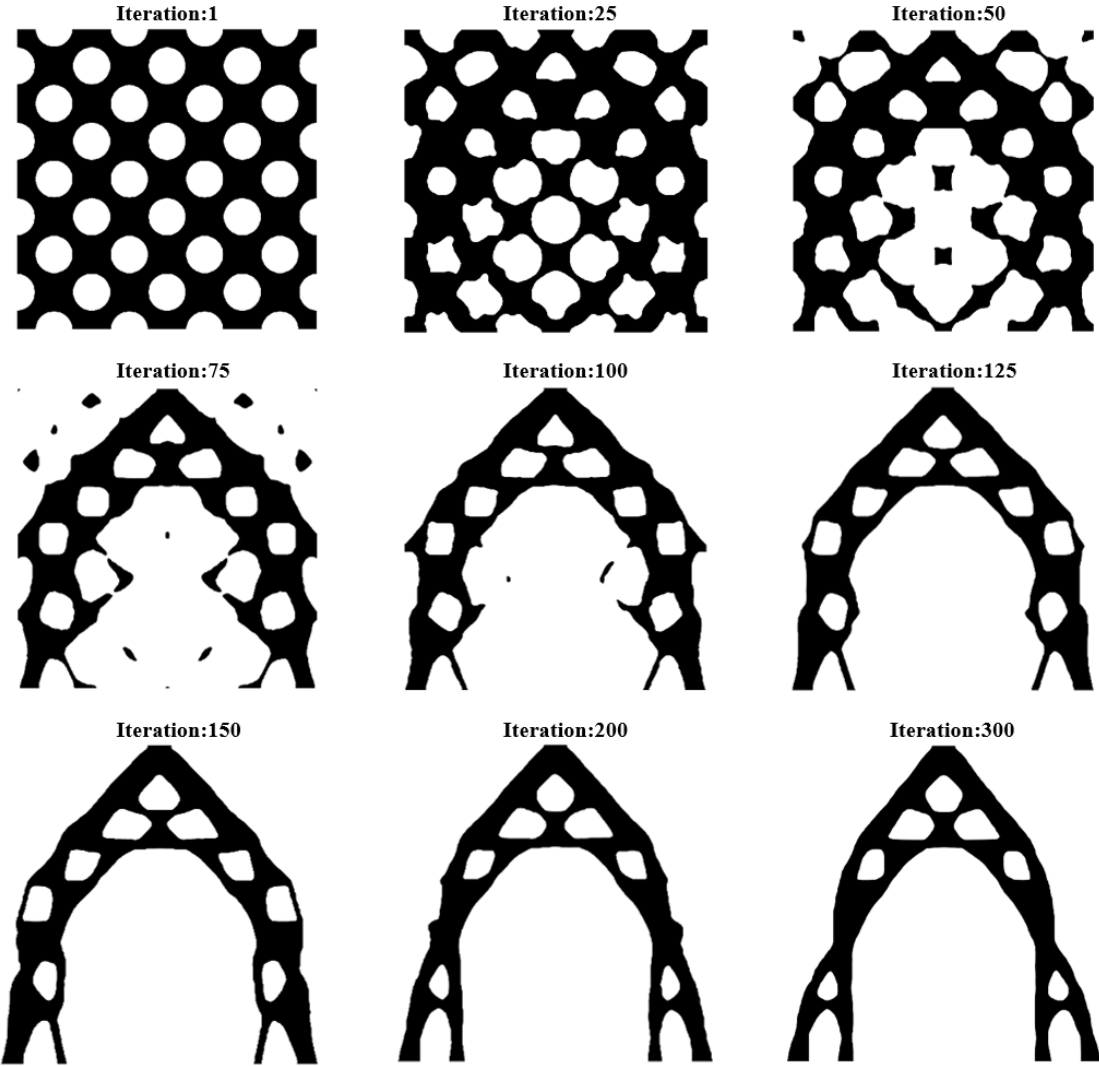


Figure 9. Evolution of material layout.

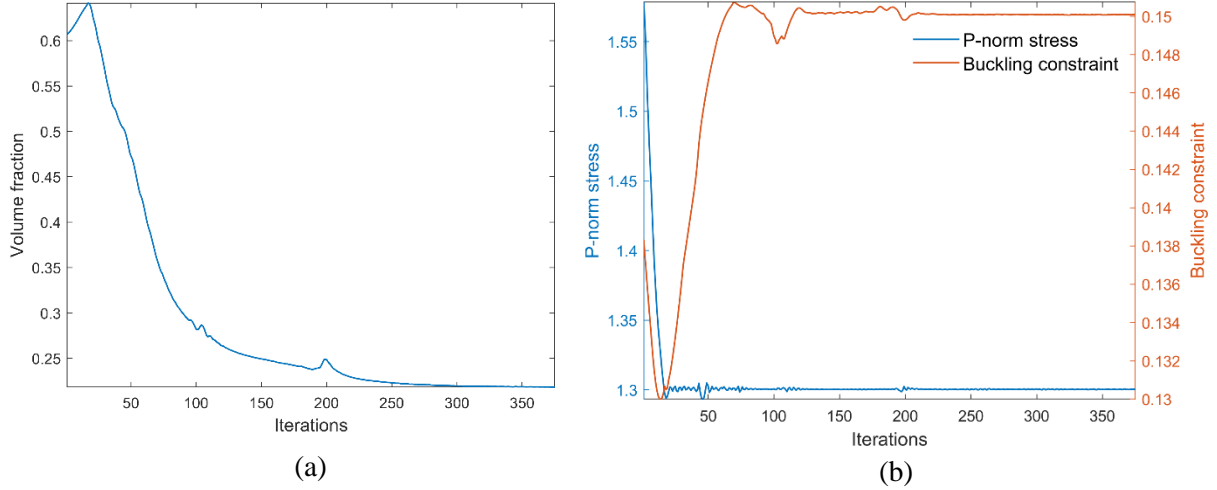


Figure 10. Convergence history. (a) objective function; (b) constraints.

4.2 L-bracket design

The dimension of L-bracket is demonstrated in Fig. 11. Note that the domain is discretized by 100×100 finite element mesh, where a 60×60 section is removed to create L-bracket domain. A vertical load $F_p = 1$ is applied on the right upper corner for stress constraint problem. For this case, the elastic modulus and Poisson's ratio are selected as: $E = 1$, $\mu = 0.3$. The B-spline velocity knots are uniformed distributed in the whole design domain as shown in Fig. 11. Assuming that the maximum length of L-bracket is L , the value of knot interval Δ is selected as $\Delta = 0.02L$. Similarly, the bounds of the velocity design variables are selected as ± 0.2 , and the moving limit of MMA algorithm is chosen as 0.2.

4.2.1 volume minimization with stress constraint

Herein volume minimization of the L-bracket model presented in Fig. 11 is explored. The P-norm stress constraint is selected as $\sigma^* = 0.65$, and the p-norm parameter is $p = 10$. The initial and optimized designs of L-bracket is plotted in Fig. 12(a) and (b), and the von-Mises stress distribution is shown in Fig. 12(c). Obviously, rounded corners are obtained in the final solution, where the final shape is much smoother than the initial design. The final optimized von-Mises stress is evenly distributed in the design space, where optimized stress distribution is close to a fully stressed design. The evolution of material layout is demonstrated in Fig. 13. As shown in Fig. 13, the boundaries of internal holes move and merge with each other, resulting a non-trivial and optimized shapes. The corresponding evolution of von-Mises distribution is plotted in Fig. 14. The optimization progress takes near 500 iterations to converge as shown in Fig. 15, where the volume fraction of optimized shape is 0.196.

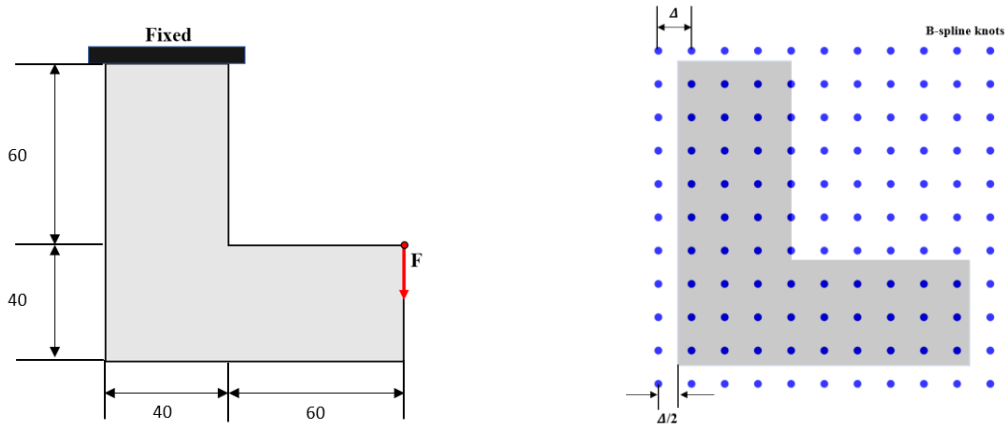


Figure 11. L-bracket design

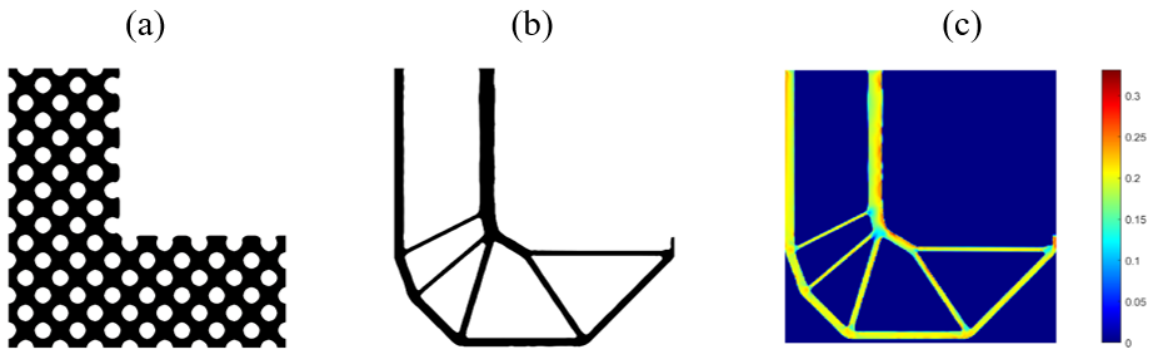


Figure 12. Volume minimization with p-norm stress constraint (a) initial design (b) optimized design (c) von Mises stress distribution

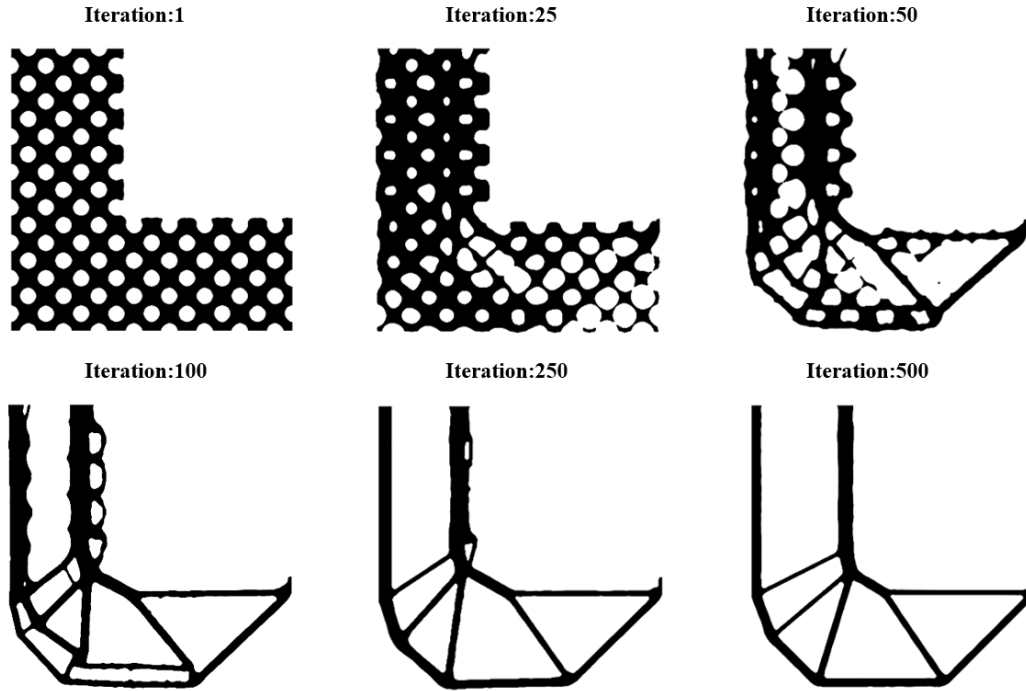


Figure 13. Evolution of material layout during optimization.

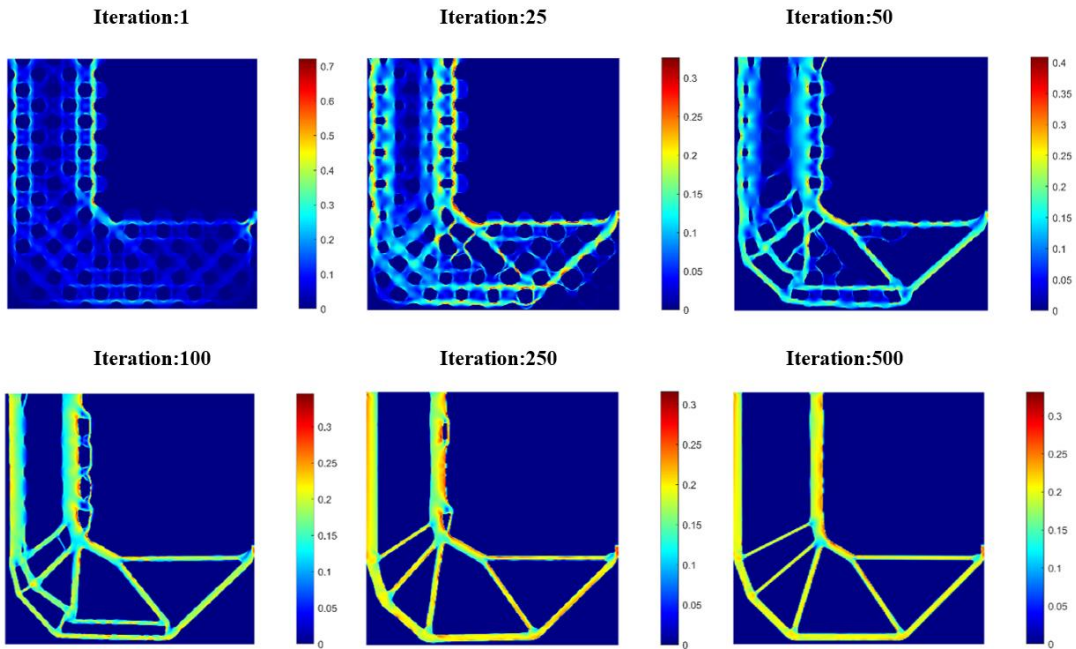


Figure 14. Evolution of von-Mises stress during optimization.

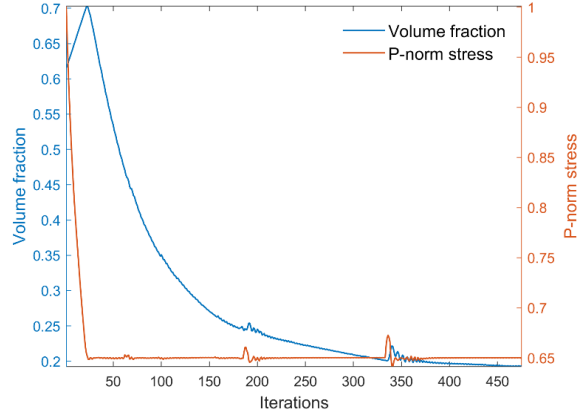


Figure 15. Convergence history.

4.2.2 Volume minimization with buckling constraint

In this section, the volume minimization of the L-bracket model with buckling constraint is investigated in the framework of proposed level set method. The finite element discretization and optimization configurations are the same as previous section 4.2.1. a downward concentrated force $F_b = 1 \times 10^{-3}$ is applied on the right upper corner. The buckling constraint μ^* is selected as $\mu^* = 2.5$. Compared with standard density-based method, the local pseudo buckling modes in the low-density regions [29] are not an issue for level set method. The initial design and optimized design are plotted in Fig. 16. In final optimized design (Fig. 16(b)), no slender bars are found, while sharp corner is inevitably generated due to no local stress constraints. Obviously, the optimized structural member in compression becomes wider to against local buckling. The volume fraction reaches 0.307 after near 700 iterations. It is worth to mention that local eigenvalues are very sensitive to boundary move and merge. Jumping phenomenon of eigenvalues may happens during optimization. Therefore, local small fluctuations are found in the convergence history (Fig. 17).



Figure 16. Volume minimization with buckling constraint (a) Initial design (b) Optimized design

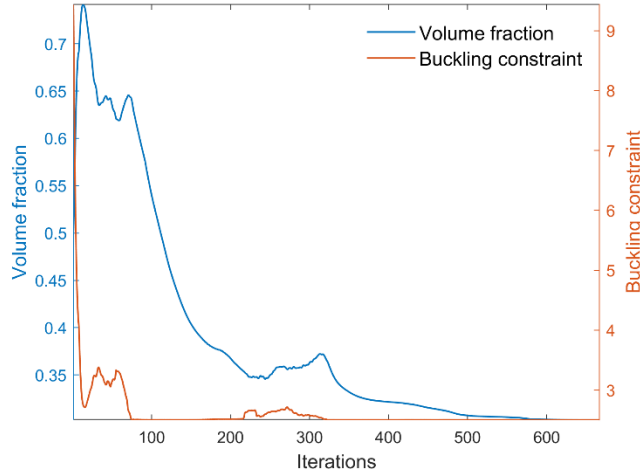


Figure 17. Convergence history

4.2.3 Volume minimization with stress and buckling constraint

In this section, the proposed methodology is applied to solve the problem with stress and buckling constraints. The L-bracket design domain is explored here. The same material properties, discretization method, and optimization configuration are implemented as section 4.2.2 and 4.2.1. Two different loading cases are applied for stress and buckling analysis. For the stress constraint case, the load force is chosen as $F_p = 1$. For the buckling case, the loading is selected as $F_b = 1 \times 10^{-3}$. Similar to section 4.2.2 and 4.2.1, the stress and buckling constraints are set as $\sigma^* = 0.65$ and $\mu^* = 2.5$. Starting with the initial design shown in Fig. 16, the solution for stress and buckling constraints is presented in Fig. 18(a). the correspondent von Mises stress field is presented in Fig. 18(b). As shown in Fig. 18(b), the maximum von Mises stress are evenly distributed nearby the rounded corner. Compared with solution in section 4.2.2, the boundary becomes smoother, and no stress concentration points are found. The minimal volume fraction obtained is 0.509. The optimization converges after near 500 iterations, and the evolution of topology shapes are demonstrated in Fig. 19.

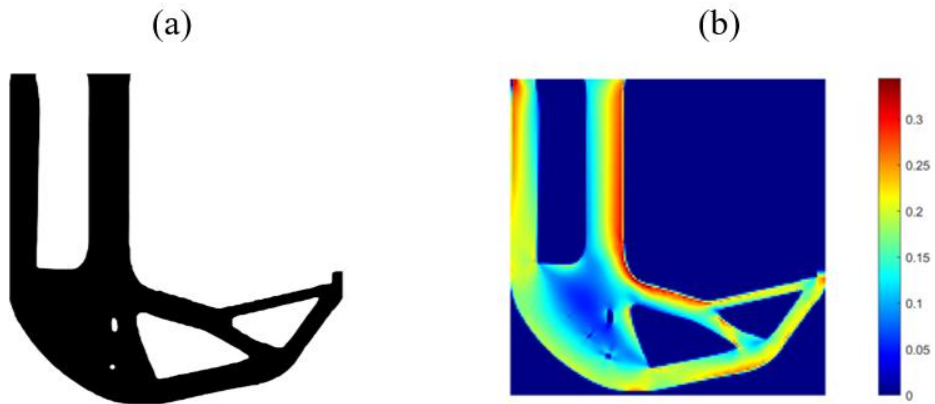


Figure 18. Volume minimization with stress and buckling constraint (a) Optimized design (b) von Mises stress distribution

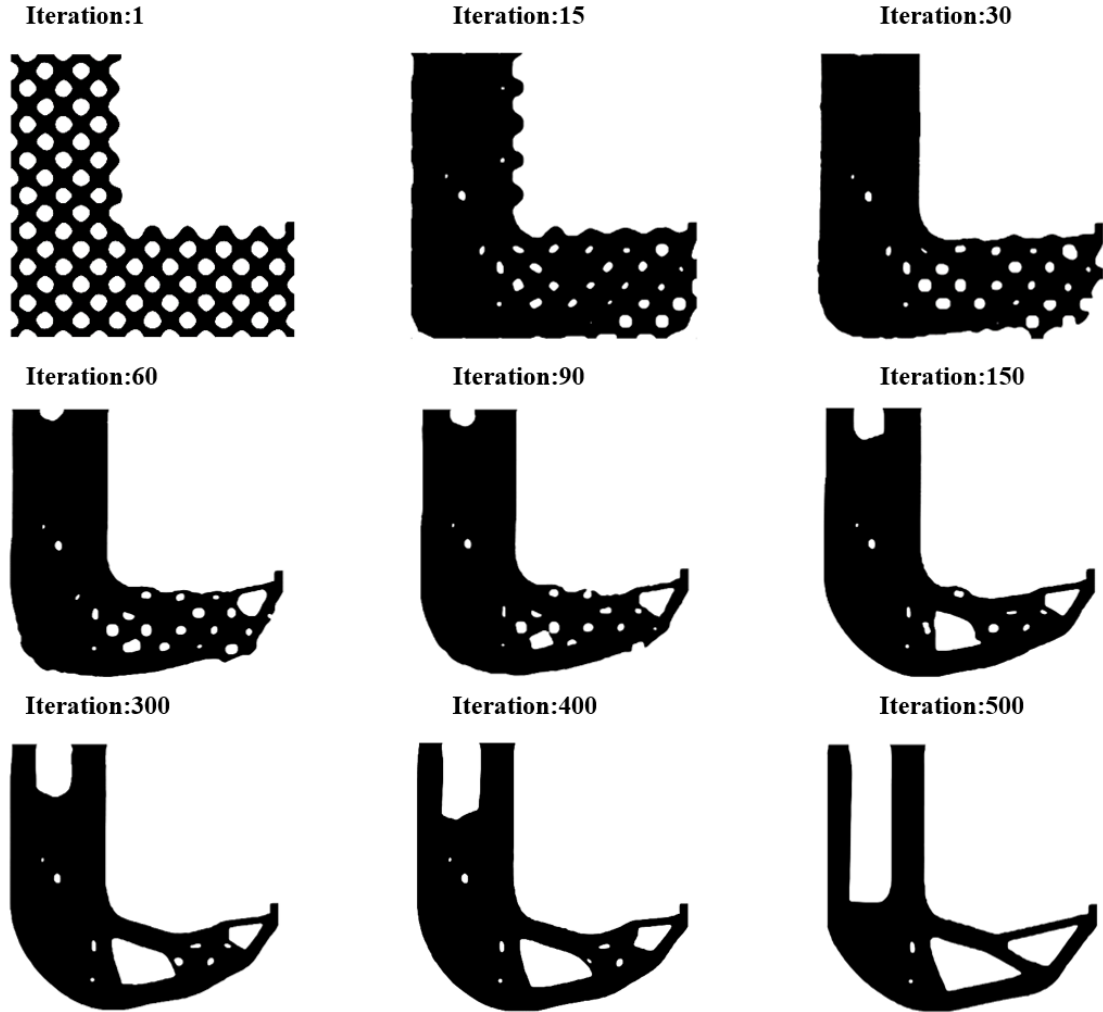


Figure 19. Evolution of material layout during optimization

4. Conclusion

In this paper, a velocity field level set (VFLS) method for topology optimization based on discrete adjoint method is presented, where the velocity field is described in the B-spline space. The analytical sensitivity of presented level set method can be fully computed using the discrete adjoint method, where the mathematical relationship between the level set velocity with discrete adjoint sensitivities are derived and demonstrated in detail. The adjoint equations are derived using the discretized governing equations. The proposed level set sensitivity analysis method does not need any smoothing or interpolation typically used in classical level set topology optimization scheme. Note that the proposed sensitivity analysis method is not limited to B-spline space, any other velocity field representation [30] can also be applied. To demonstrate the effectiveness of proposed sensitivity analysis method, stress and buckling constrained examples are presented, which are considered to be challenging in level set topology optimization. **Future work includes extending current discrete adjoint-based level set method to three dimensional problems.**

Reference

- [1] M. P. Bendsøe and N. Kikuchi, "Generating optimal topologies in structural design using a homogenization method," *Computer methods in applied mechanics and engineering*, vol. 71, pp. 197-224, 1988.
- [2] M. P. Bendsøe and O. Sigmund, "Material interpolation schemes in topology optimization," *Archive of applied mechanics*, vol. 69, pp. 635-654, 1999.
- [3] M. Y. Wang, X. Wang, and D. Guo, "A level set method for structural topology optimization," *Computer methods in applied mechanics and engineering*, vol. 192, pp. 227-246, 2003.
- [4] X. Huang and M. Xie, *Evolutionary topology optimization of continuum structures: methods and applications*: John Wiley & Sons, 2010.
- [5] X. Guo, W. Zhang, and W. Zhong, "Doing Topology Optimization Explicitly and Geometrically—A New Moving Morphable Components Based Framework," *Journal of Applied Mechanics*, vol. 81, 2014.
- [6] W. Zhang, J. Chen, X. Zhu, J. Zhou, D. Xue, X. Lei, *et al.*, "Explicit three dimensional topology optimization via Moving Morphable Void (MMV) approach," *Computer Methods in Applied Mechanics and Engineering*, vol. 322, pp. 590-614, 2017/08/01/ 2017.
- [7] W. Zhang, W. Yang, J. Zhou, D. Li, and X. Guo, "Structural topology optimization through explicit boundary evolution," *Journal of Applied Mechanics*, vol. 84, 2017.
- [8] W. Zhang, J. Yuan, J. Zhang, and X. Guo, "A new topology optimization approach based on Moving Morphable Components (MMC) and the ersatz material model," *Structural and Multidisciplinary Optimization*, vol. 53, pp. 1243-1260, 2016/06/01 2016.
- [9] J. A. Norato, B. K. Bell, and D. A. Tortorelli, "A geometry projection method for continuum-based topology optimization with discrete elements," *Computer Methods in Applied Mechanics and Engineering*, vol. 293, pp. 306-327, 2015/08/15/ 2015.
- [10] J. Norato, R. Haber, D. Tortorelli, and M. P. Bendsøe, "A geometry projection method for shape optimization," *International Journal for Numerical Methods in Engineering*, vol. 60, pp. 2289-2312, 2004.
- [11] S. Zhang, A. L. Gain, and J. A. Norato, "Stress-based topology optimization with discrete geometric components," *Computer Methods in Applied Mechanics and Engineering*, vol. 325, pp. 1-21, 2017.
- [12] N. P. Van Dijk, K. Maute, M. Langelaar, and F. Van Keulen, "Level-set methods for structural topology optimization: a review," *Structural and Multidisciplinary Optimization*, vol. 48, pp. 437-472, 2013.
- [13] G. Allaire, F. Jouve, and A.-M. Toader, "Structural optimization using sensitivity analysis and a level-set method," *Journal of computational physics*, vol. 194, pp. 363-393, 2004.
- [14] D. Adalsteinsson and J. A. Sethian, "The fast construction of extension velocities in level set methods," *Journal of Computational Physics*, vol. 148, pp. 2-22, 1999.
- [15] S. Wang and M. Y. Wang, "Radial basis functions and level set method for structural topology optimization," *International journal for numerical methods in engineering*, vol. 65, pp. 2060-2090, 2006.
- [16] Z. Luo, M. Y. Wang, S. Wang, and P. Wei, "A level set-based parameterization method for structural shape and topology optimization," *International Journal for Numerical Methods in Engineering*, vol. 76, pp. 1-26, 2008.
- [17] P. Wei and M. Y. Wang, "Piecewise constant level set method for structural topology optimization," *International Journal for Numerical Methods in Engineering*, vol. 78, pp. 379-402, 2009.
- [18] L. Jiang and S. Chen, "Parametric structural shape & topology optimization with a variational distance-regularized level set method," *Computer Methods in Applied Mechanics and Engineering*, vol. 321, pp. 316-336, 2017.
- [19] D. Guirguis, K. Hamza, M. Aly, H. Hegazi, and K. Saitou, "Multi-objective topology optimization of multi-component continuum structures via a Kriging-interpolated level set approach," *Structural and Multidisciplinary Optimization*, vol. 51, pp. 733-748, 2015.

- [20] Y. Wang, Z. Kang, and P. Liu, "Velocity field level-set method for topological shape optimization using freely distributed design variables," *International Journal for Numerical Methods in Engineering*, vol. 120, pp. 1411-1427, 2019.
- [21] Y. Wang and Z. Kang, "A velocity field level set method for shape and topology optimization," *International Journal for Numerical Methods in Engineering*, vol. 115, pp. 1315-1336, 2018.
- [22] Y. Wang, H. Yang, and Z. Kang, "Velocity field level set method incorporating topological derivatives for topology optimization," *Journal of Applied Mechanics*, vol. 89, p. 061002, 2022.
- [23] S. Kambampati, H. Chung, and H. A. Kim, "A discrete adjoint based level set topology optimization method for stress constraints," *Computer Methods in Applied Mechanics and Engineering*, vol. 377, p. 113563, 2021.
- [24] M. D. Gunzburger, *Perspectives in flow control and optimization*: SIAM, 2002.
- [25] M. P. Bendsoe and O. Sigmund, *Topology optimization: theory, methods, and applications*: Springer Science & Business Media, 2003.
- [26] M. Sarcar, K. M. Rao, and K. L. Narayan, *Computer aided design and manufacturing*: PHI Learning Pvt. Ltd., 2008.
- [27] K. Svanberg, "The method of moving asymptotes—a new method for structural optimization," *International journal for numerical methods in engineering*, vol. 24, pp. 359-373, 1987.
- [28] M. B. Giles, M. C. Duta, J.-D. Muller, and N. A. Pierce, "Algorithm developments for discrete adjoint methods," *AIAA journal*, vol. 41, pp. 198-205, 2003.
- [29] X. Gao and H. Ma, "Topology optimization of continuum structures under buckling constraints," *Computers & Structures*, vol. 157, pp. 142-152, 2015.
- [30] Y. Wang and Z. Kang, "MATLAB implementations of velocity field level set method for topology optimization: an 80-line code for 2D and a 100-line code for 3D problems," *Structural and Multidisciplinary Optimization*, vol. 64, pp. 4325-4342, 2021.
- [31] C. Le, J. Norato, T. Bruns, C. Ha, and D. Tortorelli, "Stress-based topology optimization for continua," *Structural and Multidisciplinary Optimization*, vol. 41, pp. 605-620, 2010.
- [32] R. Picelli, S. Townsend, C. Brampton, J. Norato, and H. A. Kim, "Stress-based shape and topology optimization with the level set method," *Computer methods in applied mechanics and engineering*, vol. 329, pp. 1-23, 2018.
- [33] F. Ferrari, O. Sigmund, and J. K. Guest, "Topology optimization with linearized buckling criteria in 250 lines of Matlab," *Structural and Multidisciplinary Optimization*, vol. 63, pp. 3045-3066, 2021.
- [34] F. Ferrari and O. Sigmund, "Towards solving large-scale topology optimization problems with buckling constraints at the cost of linear analyses," *Computer Methods in Applied Mechanics and Engineering*, vol. 363, p. 112911, 2020.
- [35] N. M. Poon and J. R. Martins, "An adaptive approach to constraint aggregation using adjoint sensitivity analysis," *Structural and Multidisciplinary Optimization*, vol. 34, pp. 61-73, 2007.

Appendix A. Sensitivities

A.1. Sensitivity of stress constraint based on discrete adjoint method

The discretized linear elastic equations can be written as,

$$\mathbf{K}\mathbf{u} = \mathbf{f} \quad (\text{A1})$$

where \mathbf{K} is the global stiffness matrix, \mathbf{u} is displacement vector, and \mathbf{f} is force vector. The global stiffness matrix can be assembled by elemental stiffness matrix $\mathbf{K}_{e,i}$ as follows,

$$\mathbf{K} = \sum_{i=1}^{n_e} \mathbf{K}_{e,i} \quad (\text{A2})$$

where Σ here represents the element matrix assembly operator. For density-based topology optimization, the element stiffness matrices are modeled as Ersatz material:

$$\mathbf{K}_{e,i} = (E_{min} + \rho_i(E - E_{min}))\mathbf{K}_0 \quad (\text{A3})$$

where ρ_i is the density (volume fraction) of the i th element, E_{min} is the elasticity modulus of a void element, which is a small value to avoid numerical issue, and \mathbf{K}_0 is the element stiffness matrix for unit elasticity modulus. The maximum von-mises stress can be approximated by p-norm stress [31], which can be written as,

$$\sigma^{PM} = \left(\sum_i^{n_e} \sigma_{vm,i}^p \right)^{\frac{1}{p}} \quad (\text{A4})$$

where $\sigma_{vm,i}$ is the von Mises stress of the i th element. As described in Section 2.2, the augmented Lagrangian function \mathcal{L}_p can be formulated as follows,

$$\mathcal{L}_p = \sigma^{PM} + \boldsymbol{\lambda}_p^T (\mathbf{K}\mathbf{u} - \mathbf{f}) \quad (\text{A5})$$

The adjoint vector $\boldsymbol{\lambda}_p$ can be obtained through solving $\frac{\partial \mathcal{L}_p}{\partial \mathbf{u}} = 0$. Therefore, the sensitivity of p-norm stress with respect to elemental density is given by,

$$\frac{\partial \mathcal{L}_p}{\partial \rho_i} = \frac{\partial \sigma^{PM}}{\partial \rho_i} + \boldsymbol{\lambda}_p^T \frac{\partial \mathbf{K}}{\partial \rho_i} \mathbf{u} \quad (\text{A6})$$

The detailed derivation of p-norm stress sensitivity can be found in Ref [32].

A.2 Sensitivity of buckling constraint based on discrete adjoint method

In this Appendix, the sensitivity of fundamental buckling load factor (BLF) with respect to element density is derived. Similarly, the elemental stiffness matrix can be represented by Ersatz material model as shown in Eq. (24). The fundamental buckling load factor λ_f can be formulated as Rayleigh quotient [33],

$$\lambda_f(\boldsymbol{\rho}, \mathbf{u}) = \min \left(-\frac{\mathbf{v}^T \mathbf{K}[\boldsymbol{\rho}] \mathbf{v}}{\mathbf{v}^T \mathbf{G}[\boldsymbol{\rho}, \mathbf{u}] \mathbf{v}} \right); (\mathbf{v} \in \mathbb{R}^n, \mathbf{v} \neq \mathbf{0}) \quad (\text{A7})$$

where \mathbf{G} is the global stress stiffness matrix, \mathbf{u} is the displacement vector. \mathbf{K} is the linear stiffness matrix. The general procedure of linearized buckling analysis is as follows, a) Define a reference load vector \mathbf{f} b) Compute the equilibrium displacement $\mathbf{u} = \mathbf{K}[\boldsymbol{\rho}]^{-1} \mathbf{f}$ c) Set up the stress stiffness matrix $\mathbf{G}[\mathbf{x}, \mathbf{u}(\mathbf{x})]$ d) compute the buckling load and corresponding buckling mode $(\lambda_i, \boldsymbol{\varphi}_i)$ using the following equations,

$$(\mathbf{K}(\boldsymbol{\rho}) + \lambda \mathbf{G}[\boldsymbol{\rho}, \mathbf{u}(\boldsymbol{\rho})])\boldsymbol{\varphi} = \mathbf{0}, \quad \boldsymbol{\varphi} \neq \mathbf{0} \quad (\text{A8})$$

The buckling modes are normalized such that $\boldsymbol{\varphi}_i^T \mathbf{K}[\boldsymbol{\rho}] \boldsymbol{\varphi}_j = \delta_{ij}$. Note that the sensitivity of the i th eigenvalue λ_i with respect to element density ρ_e is expressed as [34],

$$\frac{\partial \lambda}{\partial \rho_e} = \boldsymbol{\varphi}_i^T \left(\frac{\partial \mathbf{K}}{\partial \rho_e} + \lambda_i \frac{\partial \mathbf{G}}{\partial \rho_e} \right) \boldsymbol{\varphi}_i - \lambda_i \mathbf{z}_i^T \frac{\partial \mathbf{K}}{\partial \rho_e} \mathbf{u} \quad (\text{A9})$$

where \mathbf{z}_i can be obtained through solving adjoint equations,

$$\mathbf{Kz}_i = \boldsymbol{\varphi}_i^T (\nabla_{\mathbf{u}} \mathbf{G}) \boldsymbol{\varphi}_i \quad (\text{A10})$$

For local buckling constraint, an aggregation function is applied to generate a single constraint. Here, the KS function [35] is implemented as follow,

$$KS[\mu_i] = \mu_1 + \frac{1}{\gamma} \ln \left(\sum_{i=1}^q e^{\gamma(\mu_i - \mu_1)} \right) \quad (i \in \mathbb{Z}) \quad (\text{A11})$$

Note that $\mu_i = \frac{1}{\lambda_i}$, where the degree of smoothness is governed by the aggregation parameter γ . \mathbb{Z} is the set of interested μ_i . The value obtained by KS function produce an upper bound of $\max_{i \in \mathbb{Z}} |\mu_i|$. The range of parameter γ should be $[1, \infty]$. The first order derivative of KS function $KS[\mu_i]$ with respect to density ρ_e can be written as,

$$\frac{\partial KS[\mu_i]}{\partial \rho_e} = \frac{\sum_{i=1}^q \left(e^{\gamma(\mu_i - \mu_1)} \frac{\partial \mu_i}{\partial \rho_e} \right)}{\sum_{i=1}^q e^{\gamma(\mu_i - \mu_1)}} \quad (\text{A12})$$

The detailed sensitivity derivation and implementation can be found in Ref. [33].